Integrative Biology

Quantitative biosciences from nano to macro

www.rsc.org/ibiology

Volume 3 | Number 12 | December 2011 | Pages 1145–1236

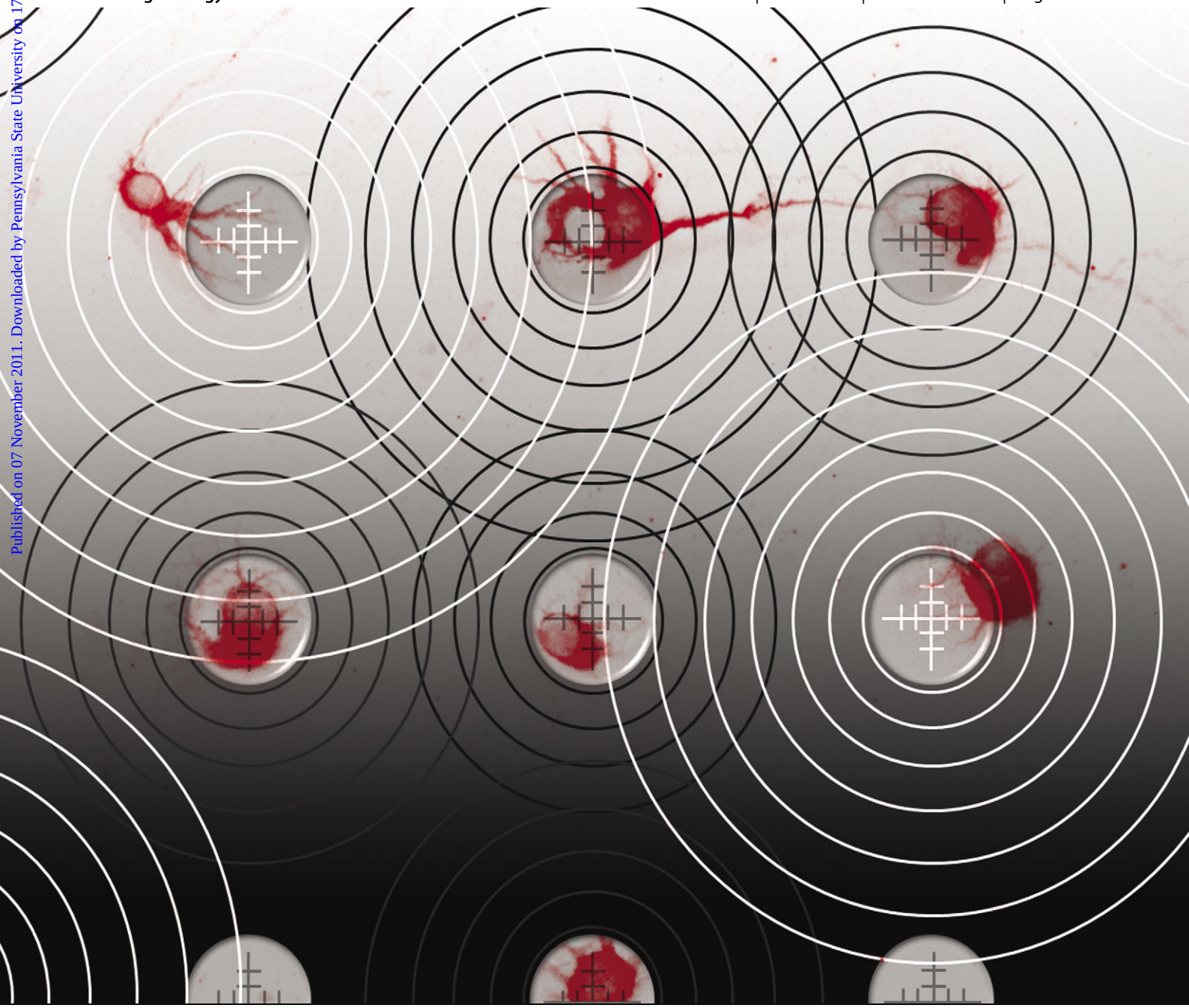

ISSN 1757-9694

RSC Publishing

PAPER

Bashir *et al.*

Pattern analysis and spatial distribution of neurons in culture

Integrative Biology

Cite this: *Integr. Biol.*, 2011, **3**, 1167–1178

www.rsc.org/ibiology

PAPER

Pattern analysis and spatial distribution of neurons in culture

Larry J. Millet,[abc] Mitchell B. Collens,[bd] George L. W. Perry[ef] and Rashid Bashir*[abd]

Received 2nd June 2011, Accepted 20th October 2011
DOI: 10.1039/c1ib00054c

The nervous system is a complex, highly-ordered, integrated network of cells. Dispersed cultures of neurons enable investigations into intrinsic cellular functions without the complexities inherent in the intact nervous system. This culture process generates a homogeneously dispersed population that is assumed to be spatially random. Despite the vast number of studies utilizing dispersed neurons, few studies address the spatial distribution of large populations of neurons, *in vitro*. We used ink-jet printing and surface chemistry to define patterned areas of poly-lysine adhesion (~50 μm spots) juxtaposed against a fluorinated-silane background. We quantitatively analysed populations of patterned neurons on printed protein spots, and unpatterned neurons. Using a microarray scanner, we acquired large images (72 mm × 22 mm) of patterns, and neurons with and without patterns. Fast Fourier transformation (FFT) image analysis was used to determine global alignment of neurons to patterns. Through point pattern analysis, we described the spatial organization of dispersed neurons with, or without, patterned substrates. Patterned neurons show spatial organization characteristics reminiscent of printed patterns, with spatial distributions representative of unpatterned neurons. Most notably, both patterned and unpatterned neurons show departure from null models of complete spatial randomness (CSR; a homogeneous Poisson process) at shorter distances with conformity to CSR occurring at longer distances. Cellular morphometrics show that when compared to their unpatterned counterparts, spot-patterned neurons exhibit a significant increase ($p < 0.0001$) in the mean dendritic circularity and an increase in the number of more circular neurons. Through neurite tracing, we show that dendritic processes are also highly confined to patterned areas, and that they are on average 58% shorter than dendrites of neurons without patterns. Our findings show that patterned areas change the spatial organization of the somata and dendrites of cultured neurons, and that traditional neuronal cultures deviate from CSR.

[a] *Department of Electrical and Computer Engineering, University of Illinois at Urbana-Champaign, Urbana, IL 61801, USA. E-mail: rbashir@illinois.edu; Fax: 217-244-6375; Tel: 217-333-3097*
[b] *Micro and Nanotechnology Laboratory, University of Illinois at Urbana-Champaign, Urbana, IL 61801, USA*
[c] *Neuroscience Program, University of Illinois at Urbana-Champaign, Urbana, IL 61801, USA*
[d] *Department of Bioengineering, University of Illinois at Urbana-Champaign, Urbana, IL 61801, USA*
[e] *School of Environment, University of Auckland, Auckland, Private Bag 92019, New Zealand*
[f] *School of Biological Sciences, University of Auckland, Auckland, Private Bag 92019, New Zealand*

Introduction

Primary neuron cultures remain an indispensible approach to advance neuroscience research. *In vitro* studies enable investigations into the inherent molecular and cellular properties of the neuron on a fundamental level, from the establishment of neuronal polarity, to synaptic plasticity,[1,2] drug development,[3,4] and neurodegenerative disease research.[5–8] An example is, the work of Banker and colleagues, who pioneered elegant research on the establishment and characterization of neuron cultures

Insight, innovation, integration

This study provides insight into the spatial distribution of neurons in cell culture. Our innovative approach uses ink-jet printing and microarray scanners to integrate pattern analysis and spatial statistics into neurobiology to resolve the large-scale spatial distribution of patterned and unpatterned neuron populations. We engineered neuronal substrates to present developing neurons with a contrast of highly-adhesive and loosely-adhesive substrates. This work is a focused study on the ability of neuronal somata and dendrites to align to engineered targets *in vitro*. A key finding of our study is that patterned and unpatterned neuron populations deviate from null models of complete spatial randomness.

demonstrating that neurons retain their characteristic morphologies in culture.[9] Other studies show that neurons in culture exhibit density-dependent viability.[10]

Understanding the characteristics of the emergent behaviour of neurons in culture is important,[6] because it has implications for the results and conclusions of the *in vitro* study. For example, common media formulations used in culturing primary neurons are under renewed scrutiny due to the bias imposed by media reagents.[11–13]

Many other questions remain unaddressed. For example, what is the spatial distribution of neurons in 2-D culture? How does the cellular distribution influence the process of differentiation and maturation within the culture? How do culture conditions, such as substrates and co-cultures, influence the spatial distribution of neurons in culture? Answering these and other fundamental, distribution- and density-dependent questions will further refine the cell culture process and advance studies that seek to resolve the intrinsic and extrinsic cellular influences.

Investigations of neurons *in vitro* have been high-resolution and low-throughput. In the former, neurons have received unprecedented exposure through dynamic imaging studies, complemented with detailed molecular and immunochemical investigations. For the latter, relatively few neurons in the cell culture population are used because imaging, counting, and classifying hundreds or thousands of cells is exhausting and time consuming.[14] Therefore, random sampling and statistical methods are often used to describe the population, treatment or condition.[14–16]

Incorporating new methods of analyses will further aid in answering these questions. The implementation of spatial statistics in cell biology has the potential to provide a greater understanding of the composition and behaviour of cellular clusters and systems that will empower cell and tissue engineering *in vitro*.

Large-scale, high resolution analyses have the potential to reveal insights into intercellular spatial relationships through multivariate analyses. Despite the decades of research on dispersed neurons in culture, there is much to be learned about the spatial order and relationship between neurons in cultures.[14–16] Here, we employ pattern analysis and spatial statistics to study the distribution of large, spatially homogeneous neuronal populations (>4000 neurons). We use inkjet printing to produce defined patterns of cell-adhesive poly-lysine; the unpatterned glass is blocked with less adhesive fluorinated-silanes. The juxtaposition of synthetic substrates provides primary neurons with a surface of contrasting physicochemical properties. Using pattern analysis and spatial statistics, we analyse substrate patterns, patterned neurons, and neurons without patterns.

Our results demonstrate that large-scale spatial analyses are able to detect the alignment of neuronal somata and dendritic fields to the patterned substrates, and that unpatterned neurons in culture can deviate from a null model of complete spatial randomness (CSR; a homogeneous Poisson process).[17] With the ability to generate large-scale patterns that influence the distribution of neurons, we can compare conventional dissociated neuron cultures with patterned cultures to add additional insight to the spatial characteristics of neurons *in vitro*.

Materials and methods

An overview of the neuron patterning process is shown in Fig. 1A. Stock glucose ink solutions are formulated to achieve 10–12 cP and $\sim$34 mN m^{-1}. Inks are then printed *via* Inkjet printing, the pattern quality is viewed by imaging the samples with a microarray scanner. Printed microscope slides are blocked with fluorinated silanes and sterilized for cell culture. Samples are prepared for cell attachment by flood coating with poly-L-lysine. Primary postnatal hippocampal neurons are cultured, fixed, labelled with antibodies, and dried. Samples are imaged with a microarray scanner and fluorescence microscope for analysis.

Ink formulation and characterization

Fluorescent proteinaceous glucose ink. A stock glucose (100–105% (w/v)) ink solution is made by dissolving 200–210 grams of glucose in 200 mL of DI water or phosphate buffered saline (PBS). Tween-20 (1% (v/v) final concentration) is added to decrease surface tension; to increase the accuracy of the final concentration, a 25% stock of Tween-20 is used for dilutions. Fluorescent proteins are diluted in the stock ink to yield printable inks, one ink contains fluorescein-conjugated poly-L-lysine (FITC-PLL), and the other contains Rhodamine-BSA (R-BSA).

Glucose ink characterization. According to the printer manufacturer, optimal inkjet printing with a Fuji-Film Dimatix DMP-2831 printer (FUJIFILM Dimatix, Santa Clara, CA) is achieved when the final ink viscosity and surface tension is between 10–12 cP and 28–30 mN m^{-1}, respectively. The viscosity is measured using a rotating cylinder viscometer (Brookfield DV II+ pro), a low viscosity cylinder (spindle 00, 20% motor power, and 22.8 C) is used to measure viscosities below 15 cP. To reduce measurement error, we use 15 mL aliquots to acquire two separate independent measurements. Surface tension is determined using a drop tensiometer (Attension Theta Lite). To reduce measurement error, the surface tension of the ink is measured four times. Fig. 1B shows the relationship between the viscosity and surface tension; values were measured during the formulation of our proteinaceous-glucose ink stock solution.

Ink-jet printing

Cleaning microscope slides. Microscope slides, 75 mm (*long*) $\times$ 25 mm (*wide*) $\times$ 1 mm (*thick*), are cleaned and prepared for ink-jet printing by either piranha cleaning or sonication. Piranha cleaning is the preferred method; slides are immersed in a 3 : 1 ratio of sulphuric acid (H_2SO_4) and 30% hydrogen peroxide (Sigma-Aldrich) for 45 min. After piranha cleaning, slides are rinsed with ethanol, dried, and cleaned with oxygen plasma. Alternatively, glass slides can be cleaned by (1) sonication in acetone (3 min), (2) rinsing with acetone, (3) sonication in ethanol (3 min), (4) rinsing with ethanol, (5) drying with nitrogen, and (6) cleaning with oxygen plasma (1 min) in a barrel etcher (Diener Pico). Either cleaning process renders the glass microscope slide hydrophilic and ready for printing.

Ink-jet printing on microscope slides. 1.5 mL of the final ink solution undergoes degassing and filtering through a 0.22 μm filter as the ink is injected into the bladder of the cartridge (Dimatix type 11610). For optimal printing results, cartridges are assembled and allowed to sit overnight in a humidified incubator (37 °C) before use.

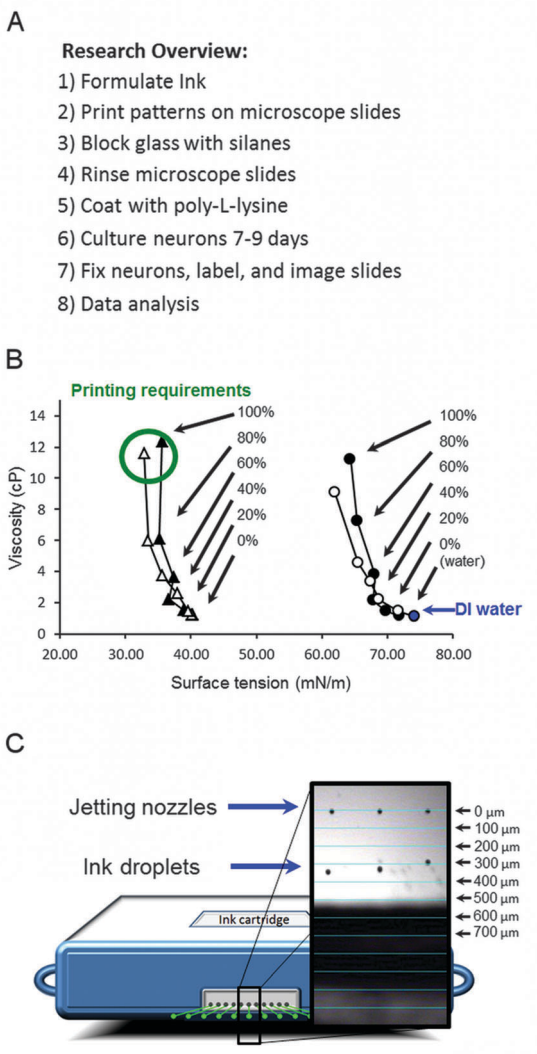

Fig. 1 Experimental overview and ink characterization. (A) A general overview of the experimental process used here. (B) Custom inks were made from a stock solution formulated to the viscosity of 10–12 cP and surface tension of 33–35 mN m^{-1}. Water and physiological saline are about 1.0 cP and 72 mN m^{-1}. Mean surface tension and viscosity values based on 4 and 2 separate measurements, respectively. Mean values are for inks with 100% glucose in the following: PBS + 1% Tween-20 (open triangles), DI water + 1% Tween-20 (filled triangles), PBS without Tween-20 (open circle), and DI water without Tween-20 (filled circles). (C) During initial setup and ink calibration, the jetting voltage of each nozzle was adjusted to ~16.0 V to optimize glucose-PBS ink droplet velocity to 6 m sec^{-1}; droplets are ~10 pL each. 6 m sec^{-1} = 300 µm/50 µs strobe delay. The inset shows an image from the drop watcher camera; the jetting nozzle holes are at the 0 µm gridline, and the droplets (shown at about the 300 µm gridline) are ejected out to the targeted surface. Below the 500 µm gridline is a shadow from the cartridge.

Droplet ejection is optimized by tuning each of the 16 nozzles with the Dimatix Drop Manager software. The target droplet (10 pL) velocity is 6.0 m sec^{-1}. The waveform editor is used to adjust the droplet characteristics to eliminate satellite droplets (Fig. 1C). Due to the thickness of the glass, the substrate height settings are set to 1000 microns. The printer platen temperature is set to 35 °C when in use.

Printed patterns are generated in the Drop Manager software. Parallel lines are best printed parallel to the *x*-axis; therefore, grid patterns are printed using two separate parallel line patterning files. First, one set of parallel lines is printed. Then the slide is rotated 90° to print the second set of grid lines. Printing spot arrays is achieved with a single printing file, but the density and complexity of the spot pattern can be adjusted to achieve different results. Nozzles can be used individually or in a set of two or more. Following inkjet printing, patterned slides are imaged on a microarray scanner to assess pattern quality before proceeding with surface chemistry.

Blocking unpatterned glass. To block unpatterned regions of the glass after printing, the patterned slides are passivated with dimethyl(3,3,3-trifluoropropyl)chlorosilane (Sigma-Aldrich) for 90 min under vacuum.[18] Specifically, three patterned microscope slides are placed in a square (90 mm × 90 mm) Petri dish along with the cap removed from a 1.5 mL micro-centrifuge tube containing 12.5 µL of silane.

Cell culture

Following the printing and passivation process, slides are prepared for cell cultures by: (1) sterilization by immersion in 70% ethanol for 30 min, (2) a brief rinsing with DI water, (3) dipping into 25 ug mL^{-1} FITC-PLL in DI water for 15 min, (4) rinsing with DI water for 10 min, and (5) rinsing with Neurobasal-A (Invitrogen) culture media.

Hippocampal neurons. Primary hippocampal neurons are cultured from postnatal (P1 to P4) Sprague Dawley rats and are used in accordance with protocols established by the University of Illinois Institutional Animal Care and Use Committee and in accordance with all state and federal regulations.

Bilateral hippocampi are dissected, prepared, and cultured as previously described.[19,20] Hibernate-A (Brain Bits, Springfield, IL) and Neurobasal-A (Invitrogen) are supplemented with 0.5 mM L-glutamine, Gem21 NeuroPlex™ (Gemini Bio-Products), 100 U mL^{-1} penicillin and 0.1 mg mL^{-1} streptomycin. Bilateral hippocampi are dissected in cold Hibernate, and incubated in papain (25.5 U mL^{-1}) dissolved in Hibernate for 30 min at 37 °C with periodic agitation. Following incubation, the tissue is rinsed with enzyme-free Hibernate and the cells are released through mechanical dissociation (trituration) with a fire-polished Pasteur pipette in 2 mL of supplemented Hibernate. After tissue chunks settle, the cell suspension is transferred to a new vial and the trituration repeated once more. Dissociated cells in solution are centrifuged at 1400 rpm for 5 min. The cells are resuspended, counted, diluted in Neurobasal media, and homogenously dispersed by plating (100–125 cells mm^{-2}) in a square 90 mm × 90 mm Petri dish containing 3 patterned microscope slides. Cultures were maintained for 7–9 days *in vitro* (DIV).

Human colorectal adenocarcinoma (HT-29) cells. HT-29 cells are cultured on poly-lysine-coated microscope slides using McCoy's 5a media supplemented with fetal bovine serum (10%) and 1% PenStrep. Cells are removed from culture flasks using trypsinization for ~5 min, dissociated with gentle

trituration, centrifuged for 5 min at 1400 rpm, suspended in culture media and plated (100 cells mm^{-2}) on poly-lysine-coated microscope slides. Cells are allowed to attach for 4 h, then samples are fixed with 4% paraformaldehyde, permeabilized with 0.25% Triton X-100, labelled with DAPI (1 : 50 000, 5 min), rinsed with DI water, dried, and imaged with a GenePix scanner.

Immunochemistry

Microscope slides containing neurons are fixed and labelled at 7–9 DIV. The samples are rinsed and fixed with pre-warmed (37 °C) 4% paraformaldehyde for 30 min. Cells are permeabilized with 0.25% Triton X-100 in PBS and blocked at room temperature with 2.5% bovine serum albumin (BSA) in PBS. Primary and secondary antibodies are incubated with 2.5% BSA in PBS. Microtubule associate proteins (MAP2 and tau) are labelled to identify axons and dendrites, respectively. Antibodies for MAP2 (Millipore, polyclonal AB5622) and tau (Anti-Tau-1 clone PC1C6, monoclonal MAB3420) are used with secondary antibodies Alexa488 and Alexa594 (Invitrogen). Following antibody labelling, samples are rinsed with PBS, briefly rinsed with DI water (to prevent salt crystal formation), dried, and imaged.

Imaging

Microscope slides are imaged with an Axon Genepix 4200A Microarray Scanner (Langer) to quickly acquire large-scale data from the microscope slide for analysis of patterns, and neurons with and without patterns. The 488 nm and 532 nm wavelength lasers are used with Alexa 488 and Texas Red filters to image labelled patterns and neurons. The Genepix 4200A scanner resolution is 5 μm/pixel. High resolution images for neurite tracing are acquired with a Spot RT-3 Slider monochrome camera (Diagnostic Instruments) mounted on an upright Olympus BX51 fluorescence microscope.

Data analysis and statistics

Global pattern analysis. Fast Fourier transform (FFT) analysis is performed on images[21] of printed patterns and patterned substrates with and without neurons. Because the FFT is a mathematical manipulation transforming spatial information to information in the frequency domain, the frequency information can be used for pattern analysis to resolve periodic changes in the pixel intensity of an image. Image J 1.44o,[22] is used for the image processing and for FFT analysis as follows. First, images are cropped to a square (2048 × 2048 pixels). Second, to limit edge effects and reduce background noise, the background is subtracted, the contrast is enhanced (0.4% saturated pixels, equalized histogram and normalized intensity), and the image is filtered with a median blur filter (two pixel radius). Third, the image is processed with the Image J FFT processing tool "FFT" to produce a 2-D image of the frequency information. The highest frequency information is located at the centre pixels of the frequency image while the lowest frequency information is in the outer pixels of the image. Fourth, the frequency image must be rotated 90° to compensate for a 90° rotation that occurs during FFT processing. Fifth, an Image J oval profile plugin is used to radially summate the frequency information to produce a power spectrum. A power spectrum is a graphical plot showing the intensity at each angle of alignment. Within the circle, 0° correlates to 3 o'clock, 90° (12 o'clock), 180° (9 o'clock), and 270° (6 o'clock).

Spatial statistics. The coordinate points of cells are derived from images acquired by a GenePix scanner. First, images are thresholded to render a binary image of cells. Background noise is filtered from the image to yield cellular points (formally "events").[23] The centroid values of each event are exported to Excel for statistical analysis. Due to the large datasets of cellular events and the limitations on spatial statistical software packages for handling large datasets, square areas (~15 mm^2) of 4000–5500 cellular events are analysed using SpPack, a Visual Basic add-in for Excel.[24]

The univariate first-order nearest neighbour (NN) test (Clark-Evans Statistic) is derived from the distance to the closest event for each data point in the spatial point pattern.[25] The test estimates the distances for nearest neighbour events under complete spatial randomness (CSR) and the departure from the observed nearest neighbour distances from those expected under a null model of CSR.[23] The ratio R is the observed NN distance divided by the expected NN distance of CSR. The edge-corrected c-score evaluates the significance of R.

The univariate second-order spatial point pattern analyses are performed using the cumulative Ripley's *K*-function and the neighbourhood density function (NDF). Ripley's *K* test provides the $K(t)$, and its linear transformation $L(t)$.[26] This cumulative test calculates (for each event) the number of events within incrementally larger radii t, along with the high and low bounds of the confidence envelope under simulations of complete spatial randomness (CSR).[24] Calculations are for 20 μm step lengths with weighted-edge corrections and a 99% confidence envelope derived from 99 Monte Carlo realisations of the null model of CSR.[27,28]

The neighbourhood density function (NDF; Ω)[29] is a non-cumulative second-order analysis that is a (rescaled) derivative of Ripley's *K*; it is analogous to the pair-correlation function. The test counts the number of cellular events within a series of annular, or O-ring, regions (x to dx) for all $x + dx$ within the plot. The counts are divided by the total area of the annuli, with the number of neighbours and area being summed for all events to yield a density function of individual events for the average event. In SpPack, the NDF is calculated with 20 μm step lengths to a maximum of 1000 μm. An edge-weighted area correction (modified from Goreaud and Pelissier)[30] is used. 99% confidence envelopes are estimated, with Monte Carlo methods, from 99 realisations of the null model of CSR.

Cellular morphometrics

Image J is used to determine the circularity of patterned and unpatterned neurons. For this data, 1 represents a perfect circle and 0 represents a line. Patterned spots, neurons cultured on spots, and randomly seeded neurons are analysed and separated into 10 bins of 0.1 intervals. Line graphs are generated and the number of neurons per circularity bin is compared using Prism statistical software using Student's *t*-test.

Neurite analysis. High resolution images (0.38 μm per pixel) of patterned and unpatterned neurons are used for local neurite analysis. Neurite tracings are performed with Neurolucida v9.62software (MBF Biosciences). Neuron reconstruction of the cell body, axon, and dendrites is completed using a semi-automated tracing technique. Tracings for all images are combined and exported to Neurolucida Explorer. Polar histograms for the patterned and unpatterned neurons are built in the Neurolucida module to display neurite directionality. The polar histogram is a 360° projection of data which accounts for neurite length and direction. In the projection, the length of a wedge is equivalent to the total length of neurite processes in a specified direction. A fan-in diagram is generated to further study axon and dendrite directionality. Statistics for determining dendritic length are performed in Prism using the unpaired *t*-test.

Results

Inkjet-printed patterns

Inkjet printing was used to produce predefined substrate patterns. To permit both the patterning of glass microscope slides and the imaging of the printed patterns, a stock ink solution was produced (100% Glucose, 1% Tween-20 in DI water) and prepared for printing with either FITC-PLL or R-BSA. Using these inks, we show that large grids, 72 mm (*l*) × 22 mm (*w*), of lines and arrays of spots can be produced on microscope slides (Fig. 2). Using the FITC-PLL ink, we patterned lines measuring 90–100 μm wide; using two different ink cartridges, we were able to print dual-labelled patterns of both FITC-PLL and R-BSA inks (Fig. 2A–C). Fig. 2A shows the entire image of a patterned grid. The details of single ink and dual ink patterns are shown (Fig. 2B–C, grid of 625 squares). We also produced printed arrays of spots using both ink formulations (Fig. 2D–F). The yield of good to perfect slides is 12% for the FITC-PLL ink (50 out of 420 printed slides) and 50% for the R-BSA ink (20 out of 40 printed slides).

Primary, postnatal hippocampal neurons were cultured for 7–9 DIV on the printed and functionalized glass (see methods). Fig. 2G shows the edge of the patterned area from one of the microscope slides where patterned neurons and unpatterned neurons are juxtaposed. Here the variation of the spatial distribution of neurons and the morphology of the dendritic field can be viewed for comparison.

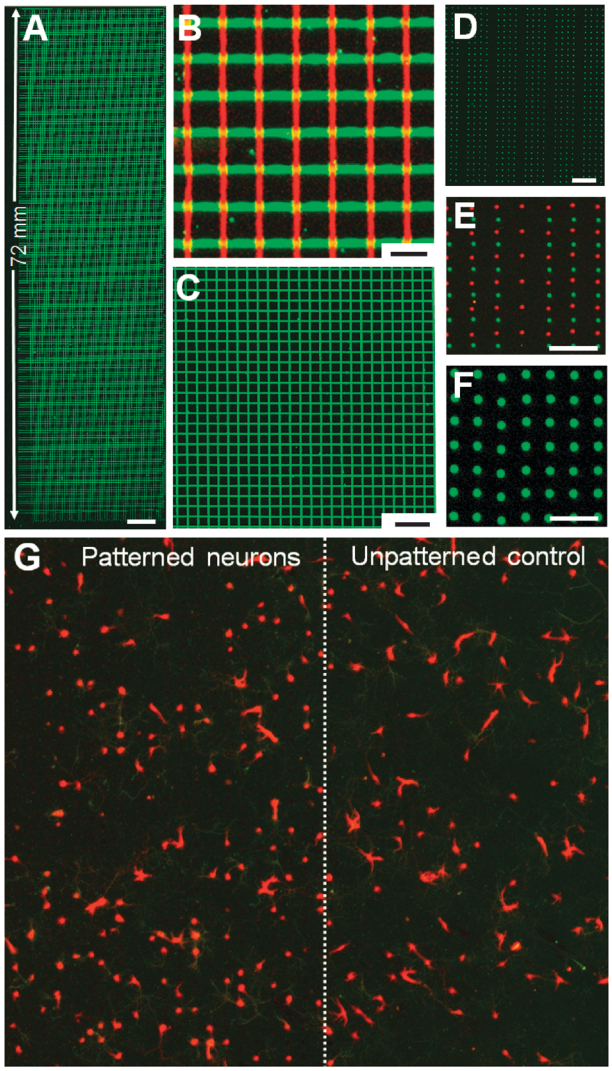

Fig. 2 Printed patterns for neuronal culture. (A–F) Large-scale patterns of fluorescein-conjugated poly-L-lysine (FITC-PLL) and rhodamine-conjugated bovine serum albumin (R-BSA) are printed using ink-jet printing. A large variety of printed patterns can be generated from lines, to grids, to arrays of spots. (G) Patterned postnatal rat neurons (P1-P2) were cultured on the spot-patterned and unpatterned glass microscope slides from (F) above. The dendrites of neurons on patterned spots are labelled with MAP2 antibodies. Patterned neurons appear to show dendritic confinement compared to neurons on adjacent internal controls (unpatterned surfaces). Scale bars are (A) 4 mm, (B) 320 μm, (C) 1 mm, (D) 1200 μm, (E) 600 μm, (F) 350 μm.

Pattern analysis

The effectiveness of the substrate to influence neuronal alignment to the patterns was determined by implementing FFT image processing methods to find the frequency and direction of patterns within the images of neurons cultured on patterned slides. For comparison, we also processed printed lines and unpatterned neurons. Fig. 3A–C shows images and the corresponding power spectrum of frequencies obtained from the FFT process of patterned spot arrays without and with cells. Distinct peaks for the coordinate axes (Fig. 3C inset, 0°, 90°, 180°, 270°) show increased frequencies of alignment for the pattern alone. For neurons cultured on spot arrays, a similar but attenuated power spectrum is obtained, whereas unpatterned neurons show no alignment.

Images and FFT data of patterned parallel lines, with and without neurons, show that neurons align to the pattern with peaks appearing at both 0° and 180° (Fig. 3D–F). The results of randomly distributed neurons without patterns show a noisy line without defined peaks, indicating no alignment for unpatterned neurons.

Spatial statistics

To characterise the spatial distribution of patterned neurons and unpatterned neurons, we used first- and second-order

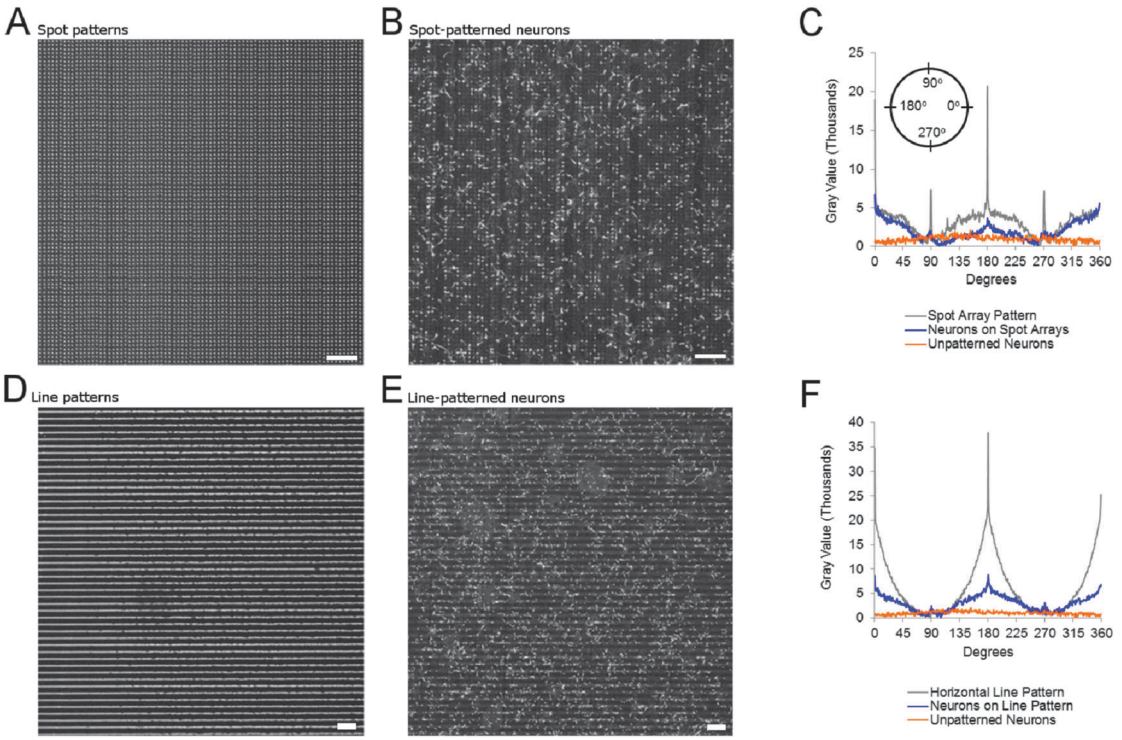

Fig. 3 Global alignment of neurons to ink-jet printed patterns. (A) Printed array of ~87 000 spots (5500 spots cm^{-2}) 45–60 μm diameter, printed with FITC-PLL ink. (B) Primary rat hippocampal neurons cultured on a patterned spot array for 9 DIV. (C) Power spectrum from 2-D FFT of spot patterns and neurons with and without patterned substrates obtained from the corresponding images. (D) Printed parallel lines 60 μm (width) × 20 mm (length). (E) Hippocampal neurons cultured on parallel line patters, 9 DIV. (F) Power spectrum from 2-D FFT of patterns, and neurons with or without patterned parallel lines for substrates obtained from the corresponding images. (C, F) Data of FFT obtained from large-scale images of panels shown here. Data for the printed patterns only (grey), patterned neurons (blue) and unpatterned neurons (orange) are quantitative analyses of the patterns and patterned neurons of the images. Power spectrums show the radial summation of the frequencies for (C) patterned spot arrays and (F) patterned parallel lines. (A-B) All scale bars are 1 mm in length.

spatial point pattern analyses. Together, the events (cellular centroids) represent a point pattern that we compare with a null model of CSR (a homogeneous Poisson process).

Results of the first-order nearest neighbour point pattern analysis show that the ratio R (observed : expected nearest neighbour distances) of the patterned neurons is greater than the ratio of the unpatterned neurons (Table 1). The c-score is significant for patterned and unpatterned neurons, but the patterned data c-scores are twice that of unpatterned neurons.

Diggles G test is a refined nearest neighbour analysis suited for testing inter-event relationships at the scale of average NN distances.[31] Fig. 4A shows the observed $\hat{G}(w)$ and the simulated $G(w)$, the cumulative proportion of nearest neighbour distances in the population. Based on $\hat{G}(w)$, the patterned neuron population appears to depart more strongly from CSR than does the unpatterned neurons. To compare the difference between the observed $\hat{G}(w)$ and theoretical $G(w)$, we subtract the $\hat{G}(w)$ from the $G(w)$ to obtain $\Delta G(w)$. By plotting $\Delta G(w)$ against the distances (w), we determine the profile of deviation from CSR for patterned and unpatterned neurons (Fig. 4B). The data shows that on average, the $\Delta G(w)$ for patterned neurons is 1.47-times greater than the $\Delta G(w)$ for unpatterned neurons.

A second-order point pattern analysis, Ripley's K, is used to determine clustering and dispersion of the spatial point pattern data. When processing the point patterns with Ripley's $K(t)$, the variance-stabilising $L(t)$ transformation shows a robust periodicity for patterned spots without neurons (Fig. 5A). The magnitude of the periodicity decreases with increasing radii distance (t), which approaches but does not converge upon CSR. Negative values below the lower boundary of the confidence envelope represent event dispersion *up to* a given distance, whereas positive values above the upper boundary represent event clustering *up to* that distance. Values within the envelope suggest no departure from CSR.

Fig. 5B shows that point patterns of neurons on printed spots have a profile and pattern similar to that observed in the $L(t)$ function of printed spot patterns without neurons. The $L(t)$ function shows periodicity in dispersion locally *up to* smaller (t) radial distances (<1000 μm), and periodicity in clustering beyond CSR *up to* larger (t) radial distances (1800 to 4000 μm). We expect that if the data were analysed with different tessellation regimes, the plot characteristics would shift toward step-wise profiles but the results would yield the same trend in conformity. In other words, regardless of the tessellation format, the patterned neuron data is expected to continue to show similar characteristics of both the printed spot patterns and unpatterned cells. For unpatterned neurons, dispersion is observed for shorter radii (<750 μm) and to a lesser degree than for patterns with and without neurons (Fig. 5C).

To determine if the data are clustered or dispersed *at* specified distances or intervals, we use the NDF, which is a

Table 1 Nearest neighbor analysis of primary hippocampal neurons

	Patterned neurons	Unpatterned neurons
Points analyzed	5199	3755
Average NN Distance	162.3 μm	178.9 μm
Average CSR Distance	135.1 μm	158.9 μm
Variance CSR Distance	1.0 μm	1.8 μm
Clark Evan's R	1.2	1.1
Clark Evan's c-score	26.3	13.5

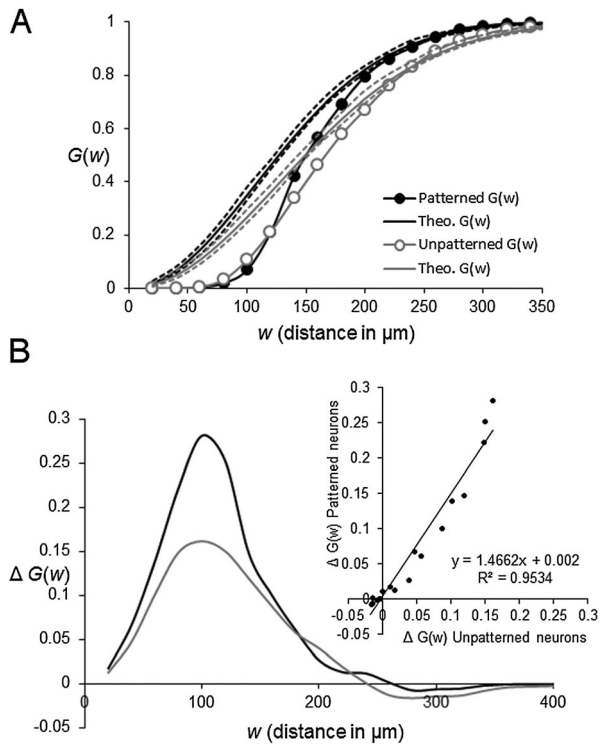

Fig. 4 First order spatial statistics. Diggle's *G* function is a first-order test that reveals the cumulative frequency distribution of events' nearest neighbour distances. (A) This analysis produces a cumulative frequency of nearest neighbour distances for cellular events with patterns (black lines with filled circles) and without patterns (grey lines with open circles). The simulated CSR is based on 99 replicate simulations and is represented by the thin smooth lines without marks positioned between the 99% confidence envelopes (dashed lines). (B) The difference between CSR and the observed data for both patterned and unpatterned neurons is shown. The following calculation gives the difference between CSR and the observed $\hat{G}(w)$, (CSR $- \hat{G}(w) = \Delta G(w)$). The greatest deviation from CSR is between 100–110 μm. The inset plot shows that the strength of departure from the model of CSR is $\sim$1.5$\times$ stronger for the patterned than the unpatterned neurons.

non-cumulative test that is more suited for exploratory analysis. As shown in Fig. 5D, the NDF of the patterned array of spots displays a periodic oscillation between clustered and dispersed, or regular, that diminishes in amplitude at further length scales. The data for the patterned neurons shows a similar, but greatly attenuated oscillation (Fig. 5E). The NDF of unpatterned neurons does not show oscillations between clustered and dispersed but resides within the 99% confidence envelope $>$150 μm (Fig. 5F); whereas $<$150 μm shows a deviation from CSR similar to that of the patterns and patterned neurons. The NDF of human colorectal adenocarcinoma cells suggests little reason to reject the null model of CSR other than a subtle departure between 50 μm and 100 μm.

Cellular morphometrics

To determine the influence of the printed spot patterns on neurons at the cellular level, we analysed the circularity values of the somatodendritic (MAP2) structure for each neuron in the population for both patterned and unpatterned neuron samples. Neurons cultured on arrays of patterned spots show a statistically significant ($p < 0.0001$, unpaired *t*-test) increase in the mean circularity above that of the unpatterned neuron population (Fig. 6). At the cellular level, there is a statistically significant ($p < 0.0001$, unpaired *t*-test) difference in the mean dendritic length of patterned neurons (267 μm) compared to unpatterned neurons (629 μm) (Fig. 7A–B). Axons and dendrites of neurons recognize the patterned cues on the glass surface. As shown in Fig. 7C, dendritic processes of neurons (7 DIV) remain confined to the patterned spots, while axons recognize the circular patterns of the spots by showing increased axonal complexity.

Discussion

Inkjet printing for cell culture substrates

Established techniques for producing patterns that direct the development of cells in culture include microcontact printing,[32] microfluidic printing,[19] and various other printing and lithographic methods.[33]

Inkjet printing has advantages that make it an attractive patterning method. Patterns of chemicals can be rapidly achieved for patterning predetermined designs without detailed photolithography or microfabrication processes. Our results demonstrate that fluorescent inks can be developed for imaging printed patterns and for generating patterns that guide neuron development in culture. Different inks can be used on the same samples for creating increasingly complex patterns (Fig. 2). By extension, inks might be used for printing patterns on topographical structures where conventional printing methods (microcontact and microfluidic deposition) would not be suitable. In addition, we envision that inks could be formulated with polymerizable hydrogel solutions for printing and encapsulating chemo-attractants and/or chemo-repellents for diffusive release. Alternatively such functionalized gels could be used as tactile signalling cues in 2-D and 3-D to control cell growth and migration, and include printed cues presented here. Through such approaches, cell-based engineering and neurobiological studies could be advanced with inkjet printing.

A wide range of studies could benefit from the advantages of inkjet printing, but the current limitations of jetting fluids must be overcome and technologies improved to advance the usefulness of this method.

In our work, we use a commercially available materials printer, the Fuji-Film Dimatix DMP-2831. The current technology of this printer has stringent physicochemical requirements for ink solutions; these specifications should be generally adhered to for optimal printer functionality and best results. Specifically, the recommended ink viscosity should be between 10–12 cP and the ideal surface tension should be about 28–30 mN m^{-1}.[34]

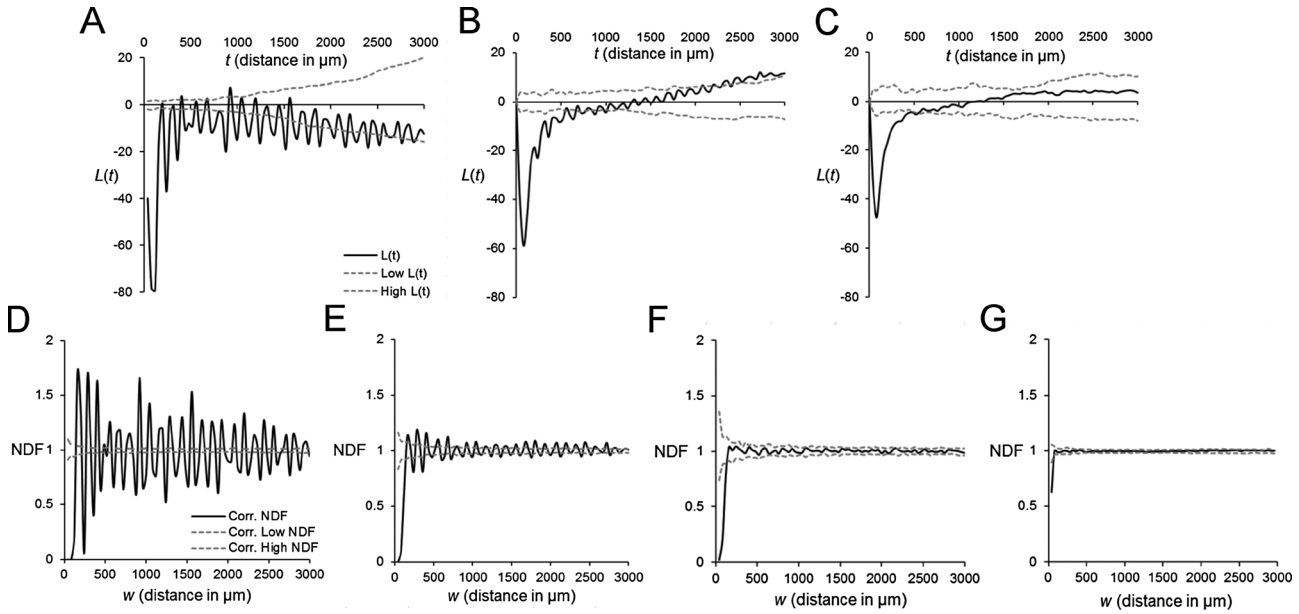

Fig. 5 Second order spatial statistics. (A–C) Ripley's *K*-function (expressed as the variance-stabilised *L*-transformation) is a cumulative second-order test that reveals aggregation and/or segregation of point patterns. When applied to our neuron data, the transform of the *K*-function reveals (A) periodic regularity and dispersion of printed patterns over 3000 μm. (B) Patterned neurons show periodic segregation or dispersion of neurons locally (<1000 μm), but aggregation or clustering globally. (C) Unpatterned neurons show similar clustering locally but without the periodicity globally. For comparison, (A–C) are plotted to the same scale. The black line is $L(t)$, which is the linear transformation of the *K*-function from Ripley's *K*-statistic, and the grey dashed lines are the 99% confidence envelopes produced from 99 simulations of CSR using the same data intensity (*i.e.* same number of points per area). (D–F) The Neighbourhood Density Function (NDF) for patterns, patterned neurons and neurons without patterns, respectively. (G) The NDF for unpatterned human colorectal adenocarcinoma (HT-29) cells.

However, the physicochemical properties of biological solutions are near that of water (about 1.0 cP and 72 mN m^{-1} at 25 °C), which are far from the specifications for controlled printing (Fig. 1). Nevertheless, for our results, the viscosity of our ink is 10–12 cP and the surface tension is 33–35 mN m^{-1}, a recipe that requires less surfactant and produces printed structures that are adequate for the surface chemistry implemented here.

In terms of user-friendly functionality, the Dimatix DMP-2831 software is easy to operate and intuitive for some operations. However, manually defining patterns for printing is extremely cumbersome and time-consuming. Importing images is possible, but the function is limited in the file types that can be accepted. Nozzle tuning for optimizing ink ejection is an advanced and beneficial function that enables precise control of droplet formation; however, even with inks that meet the physicochemical requirements, tuning the jetting of the ink is time consuming and is recommended for each cartridge.

We observe a noticeably different printing performance and yield when printing our stock glucose-tween ink (whether formulated in PBS or DI water) containing FITC-PLL or R-BSA. For FITC-PLL dissolved in the stock ink at 50 μg mL^{-1}, a 12% yield was achieved, where with the same ink stock containing R-BSA at 50 μg mL^{-1}, the yield was 50%. It should also be noted that the Dimatix DMP-2831 has a range of different cartridge types that are resistant to a variety of solvents, and jet either 1 pL or 10 pL drops. We believe that with substantial advancements in the software usability, nozzle development, and printer performance, Dimatix printers will enable greater versatility for printing physiological solutions.

Spatial distribution of neurons with and without patterns

With the ability to print and image a variety of substrate patterns, we tested the ability of synthetic substrates to guide neuron development. Studies where neuron patterning directs neuron growth often make use of biological ECM matrix compounds (*e.g.* laminin, collagen),[1,19] trophic factors (*e.g.* nerve growth factor),[35,36] or cellular ligands (*i.e.* neural cell adhesion molecules),[37] and patterned gene expression[38,39] to study the intrinsic and extrinsic influences regulating neuron differentiation, growth and maturation. Here, we use synthetic poly-lysine (PLL) and silane reagents to engineer spatially defined regions that present neurons with a contrast in cell-to-substrate adhesivity. While the influence of the pattern on the neuron is manifested in Fig. 2, the quantitative results of the FFT pattern analysis shows the global alignment of neuronal populations to the patterns compared to unpatterned control cultures (Fig. 3).

To obtain a more quantitative representation of the spatial relationships between the cellular events and the patterns, we use multiple spatial statistical tests. Using multiple tests yields the most informative perspective on the spatial distribution by complementing each other, and minimizing the limited conclusions afforded by the use of only one method. These tests, combined with the pattern analysis and cellular morphometrics, provide a thorough, quantitative, and comprehensive perspective of dissociated neuron cultures. Furthermore, these measures are useful means to discover how the spatial distribution of neurons changes with respect to patterned guidance cues.

The results of first- and second-order spatial statistics describe the spatial relationship of events within the neuronal

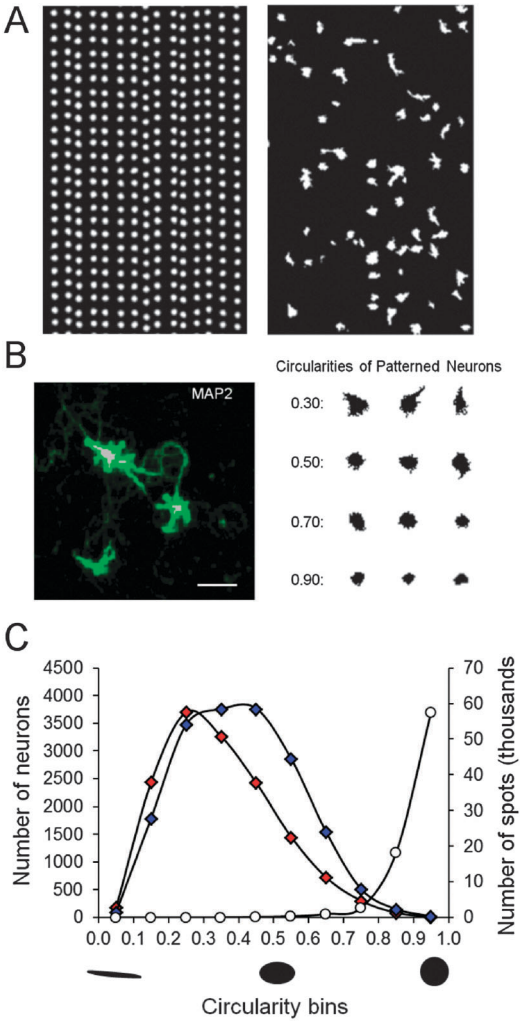

Fig. 6 Cellular morphometrics shows neuron alignment to patterns. (A) Threshold images representative of patterned spots and (B) dendritic fields (MAP2) of neurons on a patterned array of spots for deriving centroid coordinates and cellular circularities. (C) MAP2 immunochemically labelled hippocampal neurons on patterned spots and representative morphologies of cells with the respective circularities. (D) There are more circular dendritic fields on patterned substrates than on unpatterned control samples. Neuron totals are 14 000 to 16 000 per population, there is a significant difference (<0.0001, t-test) in the mean circularity between patterned (blue diamonds) and unpatterned populations (red diamonds). Scale bar = 50 μm.

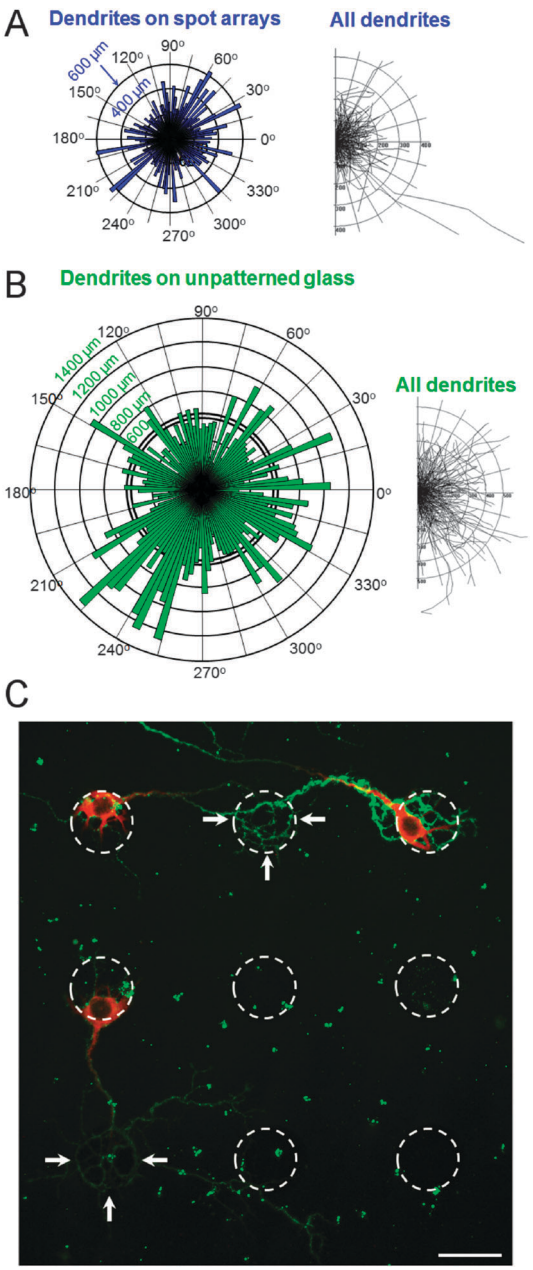

Fig. 7 Patterned neurons show dendritic confinement. (A) Hippocampal neurons cultured on patterned microscope slides (blue polar histogram) show shorter dendritic structures than (B) neurons cultured on unpatterned spots (green polar histogram). (A–B) Fan diagrams for each patterned and unpatterned dataset display the length and direction of all dendritic branches for >50 neurons. Graphs are the same scale. Rat hippocampal neurons cultured on a spot array demonstrate that both dendritic and axonal neuritis can be guided by the printed patterns. Nine spots are shown of over 87 000 spots printed per microscope slide. Spots (~50 μm dia.) defined with ink-jet printing and are outlined. Somas and dendrites (MAP2, red) are confined to spots; axons (tau, green) recognize spot patterns (arrows).

population. For first-order NN analysis, the data shows that both patterned and unpatterned neurons deviate from CSR, but the patterned neuron population departs further from CSR (Table 1). The analysis suggests the neuron populations' pattern departs from a null model of CSR, and that patterned cues intensify this departure. The null model of CSR is a valid theoretical model considering that cells in dispersed cell culture are assumed to be homogeneously dispersed when thoroughly mixed during preparation and cell plating.

We used Diggle's G refined NN analysis as a separate independent measure, which provides a relatively 'myopic' cumulative frequency of distances to the neighbouring events and to simulated CSR. That is, $G(w)$ is only really informative over length scales proportional to the mean NN distance. Fig. 4A shows increasing neuron regularity or dispersion at short distances (<400 μm). Because both patterned and unpatterned neuron data deviate from CSR, we replot the differences from CSR $\Delta G(w)$ against the distances (w) (Fig. 4B), and the deviations of both populations against each

other (Fig. 4B, inset) to determine the magnitude of the differences. Both the NN and Diggle's G analyses are in agreement that both patterned and unpatterned neurons deviate from CSR. On average the difference of the patterned population from CSR is 1.47 times greater than the unpatterned difference from CSR. In terms of analysis, not all statistical tests have the same power. Diggle's G is more suited for determining data regularity, whereas Ripley's K is more suited for determining aggregation or clustering.[23,40]

To complement the NN analyses, to better understand the spatial distribution of the patterned neurons, and to further reveal the dispersion and clustering of cells at multiple scales (t) we use second-order spatial statistics. Ripley's $L(t)$ transformation for patterns and neurons (with or without patterns) suggest dispersion *up to* radial distances of 500 μm from each cellular event. Interestingly, the data of patterns without neurons shows oscillations that traverse the lower 99% confidence envelope between dispersion and CSR (Fig. 5A). From the NN tests above, we anticipated that the pattern would influence neurons cultured on the printed cues. This influence is particularly evident when comparing the profiles for the $L(t)$ transformation data of the patterned and unpatterned neurons. The same trend away from dispersion toward CSR is observed, but the patterned neurons show a periodicity in $L(t)$ reminiscent of the printed patterns (Fig. 5B–C).

The NDF for patterns and neurons also shows characteristic oscillations. Both Ripley's K and the NDF assume first-order homogeneity, which exists in cell culture when plated evenly. The NDF is a non-cumulative test where the distance classes are annuli, or O-rings, rather than circular areas. Thus it more directly characterises spatial patterns of events in point patterns, and is more intuitive to interpret than the cumulative K-function. These combined statistical results provide evidence that the printed patterns elicit governing cues that influence the spatial distribution of neurons on patterns.

For Diggle's G, Ripley's K, and the NDF, determining the appropriate w or t value should take into consideration the error in the point position of data values, the resolution of the grid or point-to-point spacing, and it should not be courser than the average NN distances. For these reasons we analysed the printed patterns, and neurons with and without patterns using sample-relevant t values. We assume the point accuracy of the neurons to be within 30 μm, which is more than twice the average somal diameter. We also measured the noise or irregularity of the printed patterns (*i.e.* the maximum difference or variance in point-to-point position) to be 40 μm. The spot-to-spot grid spacing (mean point-to-point spacing) is 150 μm. For these reasons we analysed the data with the t-values of 30 μm, 40 μm and 150 μm. In summary, results for $t = 30$ and $t = 40$ are essentially the same; the trend also holds true for $t = 150$ with a decreased resolution and magnitude of deviation from a null model of CSR (data not shown).

Three kinds of data suggest that cell fate and neuron selection can influence neuron segregation and clustering. First, in the nervous system neurons can be, but are not always, outnumbered by glia.[41] Second, contemporary neuron culture protocols yield nearly pure neuron populations[10] by selecting against mitotic cells (*e.g.* glia and migroglia). Thus, there is an unavoidable cellular selection process inherent in the culturing primary neurons, a process that could influence the spatial distribution of neurons *in vitro*. Lastly, a deviation from CSR is further supported by the evidence that primary hippocampal and hypothalamic neurons in culture exhibit a density-dependent viability[10] and development.[42]

To test the idea that cell selection processes influence spatial distributions of cells *in vitro*, we plated cancerous cells that are not anticipated to undergo culture selection biases that are present with neurons. HT-29 Human cancerous colorectal adenocarcinoma cells show a very high, but not perfect conformity to CSR (Fig. 5G). Compared to neurons, HT-29 would retain high viability because they are gently released from the culture flasks and not harvested through mechanical tissue isolation processes. Furthermore, HT-29 would not undergo a cell selection process as cells from the brain do during serum-free neuron cultures. To minimize confounds of cell division and cell loss, HT-29 were allowed to attach for 4 h then they were processed for analysis. To what extent these conditions (*e.g.* substrates, cell selection, age of culture, *etc.*) influence the deviation of neuron populations from CSR is undetermined and will be a focus of further investigation.

Cellular morphometrics reveal dendritic confinement

In addition to spatial statistics, we also take a more conventional approach and analyse cellular alignment to the patterns. We used cellular morphometrics to determine neuronal conformity to patterned spots. The range of circularities for cellular events is shown in Fig. 6. The population shift of patterned neurons toward an increase in circularity is statistically significant (<0.0001, t-test) (Fig. 6D).

As a second measure of cellular confinement, we performed neurite tracing of the dendrites of patterned and unpatterned neurons. Hippocampal neurons cultured on patterned spot arrays show, on average, 58% shorter dendritic structures than unpatterned neurons (Fig. 7A–B). Our results suggest that dendrites of neurons not only align to the pattern, but also that their lengths are confined by it. Possible explanations for the confinement of dendrites on patterned surfaces are given in no order of preference.

One possibility is that fluorinated surfaces resist biochemical accumulation. This may inhibit the deposition of cell and media constituents on the glass surface resulting, in a lack of surface-concentrated growth factors, a condition that could delay dendritic growth.

Another possibility could be cellular and substrate-dependent adhesion biases. The fluorinated-silane surface is a factor that could promote an adhesion-selective process that determines how neurons develop or what types of neurons are retained in culture. At present there is limited research identifying what neurons are eliminated from culture, during the culture process. Substrates could have a role in biasing the retention of various neuron types. What is known is that different neuronal populations in culture can be retained based on the harvested age of the animal.[5] In summary, substrates may influence what cells are lost, and also, what cells are retained.

There is the real possibility that a combined effect of one or more of these scenarios influences how neurons are retained and how they influence the spatial deviation of the population

from CSR. Axons also demonstrate pattern recognition. In addition to pattern-dependent dendritic confinement, axons recognize the patterned spots apart from fluorinated silane surfaces. Fig. 7C shows labelled axons (tau) and dendrites (MAP2) of neurons cultured from the hippocampus. The image shows increased complexities of axonal branching when axons are in contact with the adhesive PLL spot. A recent report also shows that axons of magnocellular neurons from the hypothalamic supraoptic nucleus can present different axonal branching patterns, presumably due to different substrate cell types, and that axons in culture can develop bilaterally symmetric branching patterns when devoid of arborizing cues and confounding neural networks.[42] The observation that axons increase branching when contacting changes in substrate boundaries or geometries supports the general observation that contrast, or substrate novelty, facilitates axonal branching.[43,44]

Our data suggests that neuronal somata align to highly adhesive PLL adhesion pads which are contrasted by less adhesive fluorinated silane regions surrounding PLL pads. In the broader context, many extrinsic signals can be guidance cues to influence intrinsic cellular programs. These can be coding or non-coding cues. Coding cues confer specific signals to specific receptors or receptor classes, whereas non-coding cues have a generalized physical or chemical influence on the cell. Extrinsic cues include adhesive and non-adhesive surfaces, topography, soft or stiff substrates, and surface-bound or fluid phase chemicals. In the context of our work, we used non-coding cues that influence the spatial distribution of the neurons as neurons align to the inkjet-printed patterns, compared to the conventional approach of 'random seeded' unpatterned neurons in culture.

Conclusions

This large-scale high throughput approach combines inkjet printing, microarray scanners, pattern analysis, point pattern statistics and neurobiology to enable studies on the spatial distribution of neurons *in vitro*. By studying 4000 to 5000 neurons per spatial point pattern, through multiple tests we conclude that neuronal populations deviate from CSR locally, at shorter distances (<200 μm), but global, larger-scale analyses suggest a conformity to CSR. In reviewing previously published studies, we conclude that the technique of culturing neurons introduces a selection process that can cause the spatial distribution of cells to deviate from CSR. The underlying mechanism for a local deviation from CSR is unresolved and will be a focus of future attention. Dendritic structures are shorter and are confined by the patterned regions; axons recognize the different adhesivities of the patterned and blocked substrates.

Spatial statistical methods are widely used in the ecological and geological disciplines where the ability to repeatedly test the spatial distribution of events in point patterns is limited and temporal resolution is typically restricted to a single snapshot. We conclude that these same analyses are well suited for cell culture studies where conditions are easily controlled, reproducible, relatively quick, and time series data can be acquired. In addition, cell culture studies provide additional means to test statistical methods that can make use of data reporting on both time and space.

Acknowledgements

We thank Brian Dorvel and Piyush Bajaj for insightful discussions on surface chemistry and FFT analysis, respectively. Funding was for this study was provided by National Science Foundation (Science and Technology Center 'Emergent Behaviours of Integrated Cellular Systems' Grant CBET-0939511) and the U.S. Army Medical Research & Material Command (USAMRMC) and the Telemedicine & Advanced Technology Research Center (TATRC), under Contract #: W81XWH0810701.

References

1 G. Banker and K. Goslin, *Culturing nerve cells*, MIT Press, Cambridge, Mass., 1998.
2 L. C. Kapitein, K. W. Yau and C. C. Hoogenraad, *Methods Cell Biol.*, 2010, **97**, 111–132.
3 S. C. Barber, A. Higginbottom, R. J. Mead, S. Barber and P. J. Shaw, *Free Radical Biol. Med.*, 2009, **46**, 1127–1138.
4 G. Melli and A. Hoke, *Expert Opin. Drug Discovery*, 2009, **4**, 1035–1045.
5 G. A. Banker and W. M. Cowan, *Brain Res.*, 1977, **126**, 397–342.
6 J. Chen and K. Herrup, *Reviews in the Neurosciences*, 2008, **19**, 317–326.
7 M. M. McCarthy, *Exp. Neurol.*, 2003, **184**, 40–43.
8 R. R. Romito-DiGiacomo, H. Menegay, S. A. Cicero and K. Herrup, *J. Neurosci.*, 2007, **27**, 8496–8504.
9 G. A. Banker and W. M. Cowan, *J. Comp. Neurol.*, 1979, **187**, 469–493.
10 G. J. Brewer, J. R. Torricelli, E. K. Evege and P. J. Price, *J. Neurosci. Res.*, 1993, **35**, 567–576.
11 Y. Chen, B. Stevens, J. Chang, J. Milbrandt, B. A. Barres and J. W. Hell, *J. Neurosci. Methods*, 2008, **171**, 239–247.
12 S. Roth, S. Zhang, J. Chiu, E. K. Wirth and U. Schweizer, *J. Trace Elem. Med. Biol.*, 2010, **24**, 130–137.
13 J. van der Valk, D. Brunner, K. De Smet, A. Fex Svenningsen, P. Honegger, L. E. Knudsen, T. Lindl, J. Noraberg, A. Price, M. L. Scarino and G. Gstraunthaler, *Toxicol. in Vitro*, 2010, **24**, 1053–1063.
14 L. M. McShane and M. Palmatier, *Stat. Med.*, 1994, **13**, 523–540.
15 B. Heller, F. Schweingruber, D. Guvenc and A. Heller, *J. Neurosci. Methods*, 2001, **106**, 91–99.
16 L. M. McShane, P. S. Albert and M. A. Palmatier, *Biometrics*, 1997, **53**, 698–706.
17 J. Illian, *Statistical Analysis and Modelling of Spatial Point Patterns*, John Wiley, Chichester, England, Hoboken, NJ, 2008.
18 N. E. Sanjana and S. B. Fuller, *J. Neurosci. Methods*, 2004, **136**, 151–163.
19 L. J. Millet, M. E. Stewart, R. G. Nuzzo and M. U. Gillette, *Lab Chip*, 2010, **10**, 1525–1535.
20 L. J. Millet, M. E. Stewart, J. V. Sweedler, R. G. Nuzzo and M. U. Gillette, *Lab Chip*, 2007, **7**, 987–994.
21 C. E. Ayres, B. S. Jha, H. Meredith, J. R. Bowman, G. L. Bowlin, S. C. Henderson and D. G. Simpson, *J. Biomater. Sci., Polym. Ed.*, 2008, **19**, 603–621.
22 W. S. Rasband, *ImageJ*, U. S. National Institutes of Health, Bethesda, Maryland, USA, http://imagej.nih.gov/ij/, 1997–2011.
23 G. L. W. Perry, B. P. Miller and N. J. Enright, *Plant Ecol.*, 2006, **187**, 59–82.
24 G. L. W. Perry, *Environ. Modell. Software*, 2004, **19**, 559–569.
25 P. J. Clark and F. C. Evans, *Ecology*, 1954, **35**, 445–453.
26 B. D. Ripley, *J. R. Stat. Soc. B*, 1977, **39**, 172–212.
27 P. M. Dixon, *Encyclopedia of Environmetrics*, 2002, **3**, 1370–1383.
28 F. H. C. Marriott, *Appl. Stat.*, 1979, **28**, 75–77.
29 R. Condit, P. S. Ashton, P. Baker, S. Bunyavejchewin, S. Gunatilleke, N. Gunatilleke, S. P. Hubbell, R. B. Foster, A. Itoh, J. V. LaFrankie, H. S. Lee, E. Losos, N. Manokaran, R. Sukumar and T. Yamakura, *Science*, 2000, **288**, 1414–1418.
30 F. Goreaud and R. Pélissier, *Journal of Vegetation Science*, 1999, **10**, 433–438.
31 P. J. Diggle, *Statistical Analysis of Spatial Point Patterns*, London, UK, 2003.

32 A. P. Quist, E. Pavlovic and S. Oscarsson, *Anal. Bioanal. Chem.*, 2005, **381**, 591–600.
33 L. Gonzalez-Macia, A. Morrin, M. R. Smyth and A. J. Killard, *Analyst*, 2010, **135**, 845–867.
34 J. Sumerel, J. Lewis, A. Doraiswamy, L. F. Deravi, S. L. Sewell, A. E. Gerdon, D. W. Wright and R. J. Narayan, *Biotechnol. J.*, 2006, **1**, 976–987.
35 N. Gomez, Y. Lu, S. Chen and C. E. Schmidt, *Biomaterials*, 2007, **28**, 271–284.
36 L. M. Yu, J. H. Wosnick and M. S. Shoichet, *J. Neurosci. Methods*, 2008, **171**, 253–263.
37 T. Esch, V. Lemmon and G. Banker, *J. Neurosci.*, 1999, **19**, 6417–6426.
38 P. M. Heron, B. M. Sutton, G. M. Curinga, G. M. Smith and D. M. Snow, *J. Neurosci. Methods*, 2007, **159**, 203–214.
39 T. Houchin-Ray, A. Huang, E. R. West, M. Zelivyanskaya and L. D. Shea, *J. Neurosci. Res.*, 2009, **87**, 844–856.
40 S. Barot, J. Gignoux and J. C. Menaut, *Ecology*, 1999, **80**, 1987–2005.
41 C. C. Hilgetag and H. Barbas, *Brain Structure and Function*, 2009, **213**, 365–366.
42 L. J. Millet, A. Bora, J. V. Sweedler and M. U. Gillette, *ACS Chem. Neurosci.*, 2010, **1**, 36–48.
43 D. W. Burmeister and D. J. Goldberg, *J. Neurosci.*, 1988, **8**, 3151–3159.
44 G. S. Withers, C. D. James, C. E. Kingman, H. G. Craighead and G. A. Banker, *J. Neurobiol.*, 2006, **66**, 1183–1194.